
Automated Quantitation of Three-Dimensional Cardiac Positron Emission Tomography for Routine Clinical Use

Keri Hicks, Girija Ganti, Nizar Mullani, and K. Lance Gould

Division of Cardiology in the Department of Medicine and the Positron Diagnostic and Research Center, University of Texas Health Science Center, Houston, Texas

Visual comparison of rest/stress cardiac positron emission tomography indicates coronary flow reserve for diagnosing and assessing severity of coronary artery disease. An accurate, rapid, automated method for comparison and quantitation of paired cardiac PET studies has been developed to analyze size, intensity, statistical significance of and changes in perfusion or metabolism. The method utilizes polar coordinate maps derived from circumferential profiles of true short axis slices; from the short axis data algorithms determine mean and minimum activity levels in the anterior, septal, lateral, inferior and apical regions of the myocardium, percent of the cardiac image in specific ranges of activity levels or their changes and the percent of myocardium beyond 1.5, 2.0, and 2.5 standard deviations from the normal range with blackout display of the areas beyond these statistical limits for rest, stress, and stress/rest ratio polar maps. Additional applications include comparing stress-stress images to evaluate progression/regression of stenoses, early and late resting rubidium images for determining myocardial viability based on rubidium washout kinetics, and perfusion-metabolic comparisons for quantifying ischemia, viability and necrosis after acute myocardial infarction.

J Nucl Med 30:1787-1797, 1989

Visual interpretation of rest-stress positron emission tomography (PET) using rubidium-82 (^{82}Rb) or nitrogen-13 (^{13}N) ammonia has a high sensitivity and specificity of 95-98% for the diagnosis of significant coronary artery disease (CAD) by comparison to coronary arteriography (1-5). Visual defect severity correlates with severity of coronary artery stenosis by quantitative coronary arteriography in which all stenosis dimensions of percent narrowing, absolute lumen area, and integrated length are taken into account (4). Quantitation of relative decreased activity in visually outlined perfusion defects also correlates with arteriographic severity of stenoses (6). However, the visual-interactive algorithm for this quantitation requires intense operator interaction, time, and judgement to draw regions of interest (ROIs) in multiple views of multiple tomographic slices of combined rest-stress studies (6). It is therefore subject to observer bias and is difficult to use clinically.

Accordingly, an accurate, rapid, automated routine

method was developed for quantitatively analyzing the size, intensity, statistical significance of, and quantitative changes in activity distribution of cardiac PET images for clinical and investigative applications. This report describes the method which automatically derives regionally (a) the most severe perfusion defect or minimum activity expressed as a percent of normal areas, (b) the average intensity of myocardial regions as a percent of normal areas, (c) the percent of the heart image that is 1.5, 2.0, and 2.5 s.d.s away from the mean of 30 normals, and (d) the percent of the heart image within 20% increments of activity levels from 0% to 100% (normal). All of these measurements are automatically obtained for each quadrant and apex of the rest image, the stress image, the ratio image of absolute activity at stress divided by absolute activity at rest (an image of absolute perfusion reserve) and finally the ratio of relative stress activity distribution divided by relative resting distribution (an image of the change in relative perfusion reserve).

Preliminary data from this method are described for the following applications: (a) rest-stress PET for the diagnosis, localization and severity of coronary artery disease, (b) sequential stress-stress image comparisons

Received Dec. 30, 1988.; revision accepted July 21, 1989.

For reprints contact: K. Lance Gould, MD, Div. of Cardiology, P.D.R.C., 4.258 MSMB, University of Texas Medical School at Houston, P. O. Box 20708, Houston, TX 77225.

for following changes in stenoses, (c) comparison of stress perfusion-metabolic studies to quantitate viability necrosis or stress-induced ischemia, (d) comparison of early (first 90 sec of data) and late images after a single resting injection of generator produced ^{82}Rb to determine arterial patency and myocardial viability after myocardial infarct or thrombolysis.

METHODS

Positron Emission Tomography

Patients were fasted for 8 hr and caffeine, theophylline, and cigarettes were withheld for 8 hr prior to study. Fluoroscopy was used to mark the cardiac borders for patient positioning. Scans were performed using the first prototype University of Texas multi-slice tomograph with a reconstructed resolution of 12 mm full width at half maximum (FWHM) inplane and 14 mm FWHM axially. Transmission images were performed to correct for photon attenuation. Emission images were obtained following i.v. injection of generator-produced ^{82}Rb or cyclotron produced nitrogen-13 (^{13}N) ammonia (2,4). To allow for blood-pool clearance, there was a 15- to 60-sec delay after completing the infusion of ^{82}Rb depending on the age of the generator. For a fresh generator the concentration of activity is high thereby making the infusion period shorter, more circumscribed and therefore less time is needed for blood-pool clearance. There was a 3-min delay after ammonia administration. Data was acquired for 5 to 7 min for ^{82}Rb and 15 to 20 min for [^{13}N]ammonia.

At 10 min after administration of the first dose of ^{82}Rb or 40 min after [^{13}N]ammonia, dipyridamole (0.142 mg/kg/min) was infused for 4 min. Two minutes after the infusion was completed, 25% of the pre-determined maximal handgrip was held with one hand for 4 min. Two minutes after starting the handgrip, a second dose of the same amount of the same tracer was injected, and imaging was repeated. For those patients developing significant angina, aminophylline (125 mg) was given intravenously.

Transmission scans contained 200 to 400 million counts. Emission scans contained 10 to 25 million counts for 40 to 50 mCi of ^{82}Rb and 20 to 40 million counts for 15 to 20 mCi of [^{13}N]ammonia.

Three-Dimensional Restructuring Algorithm

The set of transaxial cardiac images obtained from PET is oriented in a transverse plane perpendicular to the axis of the body. Since the heart is positioned with its long axis to the left and downward relative to the body axis, the transverse slices are not oriented for the most advantageous analysis. For effective quantification, the transaxial or acquisition data is restructured into slices perpendicular to the long axis of the heart, called short-axis views.

In generating short-axis views, the PET operator marks a line bisecting the left ventricle (LV) in a midventricular slice thereby defining the long axis of the LV. The angle between this line and the vertical is the z-axis angle of rotation. The PET operator then positions a 64-pixel square ROI around the heart of a mid-ventricular transaxial image. The user-friendly routine automatically extracts the selected region from each of the transaxial images and places the data into

the appropriate XY planes of a 64-cubic pixel array. Taking the slice separation distance and pixel size into account, additional slices are interpolated between the original transaxial planes in the z-direction to fill the central portion of the 64-cubic pixel array with 33 XY planes of data. Using a three-dimensional restructuring algorithm, the 64-cubic pixel array is rotated by the measured z-axis angle to produce a set of mid-ventricular slices in planes perpendicular to the transaxial imaging planes. The PET operator then selects a rotated mid-ventricular slice and marks a line bisecting the LV which defines the vertical angle. The angle between this line and the horizontal is the x-axis angle of rotation.

The 64-cubic pixel array containing the original transaxial and interpolated slice data is rotated once by the measured z-axis and x-axis angles of rotation using the three-dimensional restructuring algorithm. The rotated array is then reordered to place the true short axis views in the XY planes of the cube. By default, the 64-cubic pixel data set contains the long-axis views of the LV in the XZ and YZ planes. The three-dimensional restructuring algorithm for generating true short and long axis views from PET transaxial cardiac images was validated by testing with computer generated and phantom data sets. Only 11 sec of CPU time of a VAX 11-780 (Digital Equipment Corp.) are required per rotation, and accurate, with only one rotation and two interpolations required to generate short axis views, as shown in results.

Polar Coordinate Map Computation

Restructured short-axis views serve as input data to a routine which computes polar coordinate maps for rest and stress images by a method based on that reported for single photon emission computed tomography (SPECT) imaging (7,8). From 64 short-axis views, a user selects the apex of the heart from which the algorithm automatically selects 15 additional short-axis views at one-half centimeter intervals along the true long axis up to the base of the heart. The center of the left ventricular cavity and a radius of search are determined by analysis of an averaged image computed by summing the set of 16 short-axis views. Circumferential profiles are automatically generated for each short-axis view, excepting the most apical, by an algorithm which divides each view into 40 equal sectors each encompassing 9° , identifies all pixels with values in the top 2% of each sector, averages them and displays those pixels as the normal reference areas of 100% activity. The algorithm searches the apical view for the mean top 2% of data that is assigned to the centermost region of the polar map. Use of the mean upper 2% of intensity values rather than the maximum value reduces the effect of statistical noise. In the two-dimensional polar map, the circumferential profiles are arranged as a series of concentric circles with the apex of the heart corresponding to the center of the polar representation and the outermost circle corresponding to the most basal slice.

Comparative Analysis of Rest and Stress Studies

A set of four specialized polar coordinate maps reflecting regional activity distribution at rest and stress, the change in absolute activity and change in relative distribution rest to stress is created utilizing rest and stress polar coordinate maps as input. Two of the four specialized polar maps are scaled from 0% to maximum activity, 100%, in order to reflect relative regional distribution of activity throughout the myo-

cardium during rest and stress on the same scale. These two "scaled" polar maps are produced by an algorithm which searches the original rest and stress polar coordinates for maximum activity and determines the average of the top 5% of the activity values. The routine assigns a value of 100% to the regions where activity is equal to or greater than the average maximum value and computes values for all other regions of the scaled polar maps using the equation: Scaled activity value = (Activity value/maximum activity value) × 100. These scaled polar maps are displayed by grouping the scaled activity values into ranges of 5% with a discrete color scale which uses one color to represent each five percent of activity.

An absolute ratio polar map is computed by an algorithm using original rest and stress polar coordinate maps as input data, normalizes the two maps to compensate for differences in injected dose, and produces a ratio map by dividing the values of the dose corrected stress polar map by those of the dose corrected rest polar map. The routine corrects for widely deviant rest and stress data, such as wild points caused by misregistration at the edge of the image, by setting any ratio above 2.0 to 2.0, since the maximal increase in radionuclide uptake for a fivefold flow increase would be approximately two because extraction of perfusion tracers fall by a factor of 2.5 to 3 for a 5 times increase in flow (9-11).

The relative ratio polar map shows the relative regional change in activity from the scaled rest to stress images. It is generated by an algorithm which divides the values of the stress scaled polar map (0 to 100%) by the values of the rest scaled polar map (0 to 100%) producing relative ratio values on a scale of 0.0 to 2.0 with the same restriction on widely deviant relative ratio values.

Quantitative Analysis of Regional Activity

In order to quantitate relative regional activity, all polar maps are divided into fixed sections representing the lateral, anterior, septal, inferior, and apical quadrant of the polar display. The basal portion of the data, corresponding to the atrioventricular ring or outer circumferential rim of the polar map, is excluded from the quantitative analysis because the basal portions of the polar maps contain more statistically deviant data than the other portions that adversely affect statistical analysis.

A minimum algorithm for each quadrant of each polar map determines the lowest average 5% of the data as the regional minimum activity value. The mean algorithm determines, for each of the polar maps, the mean activity level in each of the five regions.

A fractionation routine provides the percent of the cardiac image with given relative activity levels for each of the specialized polar maps. In order to eliminate the geometric distortion inherent in polar displays, the circumferential profiles from true short-axis views that define the polar maps serve as input to the fractionation routine. The algorithm scans the rest and stress scaled circumferential profile values counting the number of profile values in the ranges of 0 to 20%, 21 to 40%, 41 to 60%, 61 to 80%, and 81 to 100% of normal (maximum) activity. The number of profile values within each range is divided by the total number of profile values to produce five fractions describing the frequency of specific activity levels in each scaled polar map. Next, the fractionation routine searches the absolute ratio map profile values deter-

mining the number of profile values in the ranges 0.1 to 0.9, 0.9 to 1.1, 1.1 to 1.25, 1.25 to 1.4, and 1.4 to 2.0. The values in each range are divided by the total number of profile values in the map to give five fractions detailing the change in these activity ranges from rest to stress. Finally, the algorithm searches the relative ratio map profile values, totaling the number of profile values in the ranges < 0.33, 0.33 to 0.66, 0.66 to 1.0 and 1.0 to 2.0, and computes four fractions which describe the change in these ranges of activity from rest to stress.

Statistical Analysis for Significance of Abnormalities

The s.d. blackout routine automatically identifies regions for each polar maps which have values that deviate significantly from standard normal values based on studies of thirty disease-free individuals. The blackout algorithm creates standard deviation blackout polar maps by performing sector-by-sector comparisons of polar map images from an individual study with sets of normal s.d. images of 1.5, 2.0, and 2.5 s.d. The blackout routine then computes the percent of circumferential profile units which are blacked out in the lateral, anterior, septal, inferior, and apical regions of each of the s.d. polar maps. Thus, the percent of the cardiac image that falls beyond 1.5, 2.0, 2.5 s.d. from normal is automatically determined regionally and for the whole heart for each of the four specialized polar maps.

Display and User Interaction

A user-friendly, menu-driven program displays essential visual and quantitative information by a single command key. Rest and stress transverse, long and short axis, and polar coordinate map image sets are displayed with a selectable format for a complete study presentation or slice-by-slice comparison on the three video planes of the monitor. The intensities of rest and stress paired slice sets can be independently altered without affecting the automated quantitative routines. The scaled, absolute ratio, and relative ratio polar maps are displayed along with related quantitative information on the same video screen as the long-axis views and original polar coordinate maps. With button functions, the user can select any of the quantitative information, minima, means and fractional breakdowns, for display on the screen next to the appropriate polar map. The display routine allows the user to overwrite the four specialized polar maps with a chosen set of s.d. (1.5, 2.0, or 2.5) blackout polar maps. The percent of blacked-out profile units in a region for the selected standard deviation is written to the screen next to the appropriate blackout polar maps.

The display program has a routine for entering into the display a visual interpretation of the study for the scaled, absolute ratio and relative ratio polar maps. The user is prompted by a simple screen menu to enter codes describing visual intensity and size of abnormalities in each region and over the entire map for each of the four polar maps. After visual interpretation is completed, the display routine prompts the user to enter clinical information which, with visual interpretations, is written to a record file that can be accessed by statistical and database routines. The comprehensive display and cardiac restructuring routines form a highly integrated software package for generating, analyzing, storing and recalling short- and long-axis views, polar coordinate maps, and quantitative data with a minimum amount of user interaction.

The entire analysis including display of all quantitative data and visual interpretation can be carried out in 2 to 5 min depending on the speed of visual interpretation.

Error Analysis of ROI Statistics for the Three-Dimensional Restructuring Algorithm

Error analysis was made to measure the errors introduced into a data set by interpolation procedures. Specifically, this analysis examined the errors introduced by expanding a square region (40×40 , 50×50 , 60×60) of original image data to create a 128×128 image composed of original data interspersed with linearly interpolated data.

Twenty cardiac images were randomly selected as input data for the error analysis. For this study, the dimensions of the square section positioned around the heart were limited to one of three sizes: 40×40 , 50×50 , or 60×60 . After the rotation angle and square section are marked, a rotate-test algorithm computes a set of rotated myocardial images. The user selects one myocardial image from the set and the program initiates an interactive ROI drawing routine. The ROI is a variable size square which the user positions at a location of interest (i.e., midwall, apical edge, LV cavity edge, lateral edge, septal edge) and the program computes the number of pixels and the average pixel value in the ROI using, initially, only the actual original data contained in the ROI and, second, all data, original and interpolated, contained in the ROI. Five ROIs were drawn for each of the 20 cardiac images selected for analysis. The data from the selected ROIs were written to a file which provided the input for the program ROI-status. ROI-status determines the percent error, for all the data. The program also computed average percent errors for data from ROIs of specific size and location.

RESULTS

Error analysis showed that the average percent error computed from all ROI data after three-dimensional rotation was 2.36%. Average percent errors based on ROI location and size were also calculated. The average percent error in midwall regions was 1.05%, while in edge regions (apical, left ventricular cavity, lateral, and septal areas of myocardium), it increased to 3.24%. Every percent error in the data set which was $>5\%$ was from an edge region ROI with 17% being the largest percent error, located in an edge area. Ten of twelve ROIs with less than 10 pixels contained only one original pixel. Consequently the average percent error for ROIs with <10 pixels and with 10 or more pixels was determined. For ROIs with <10 pixels, the average percent error was 4.29%, while the average percent error for ROIs containing 10 or more pixels was 2.10%. Thus, the average percent error increased by a factor of 2 when the ROI size was <10 pixels.

Accordingly, data in a ROI taken from a myocardial image which has been rotated and interpolated once in three dimensions will have a value that is on the average within 2.36% of the value in the comparable region of interest from the original cardiac image. For quantitative analysis no ROIs containing <20 pixels was utilized and edge regions were excluded from the quantitative

analysis of polar coordinate maps carried out after rotation. Consequently the actual error is considerably $<2.36\%$. Images were reconstructed at 12 mm FWHM with 1 pixel equalling 2.5 mm or 4 pixels per linear centimeter, or 16 pixels per cubic centimeter. Partial volume errors are minimized by quantifying midwall peak (average top 2%) activity profiles for relative distribution, relative ratios or changes in activity.

Figure 1 shows the orientation of cardiac tomographic image planes viewed as if looking down from above on one's own sectioned heart. Tomographs of vertical hearts tend to be doughnut shaped whereas in horizontal hearts they are horseshoe shaped.

Figure 2 shows the distribution of the coronary arteries as viewed from above with the vascular bed of the left anterior descending coronary artery at the top of

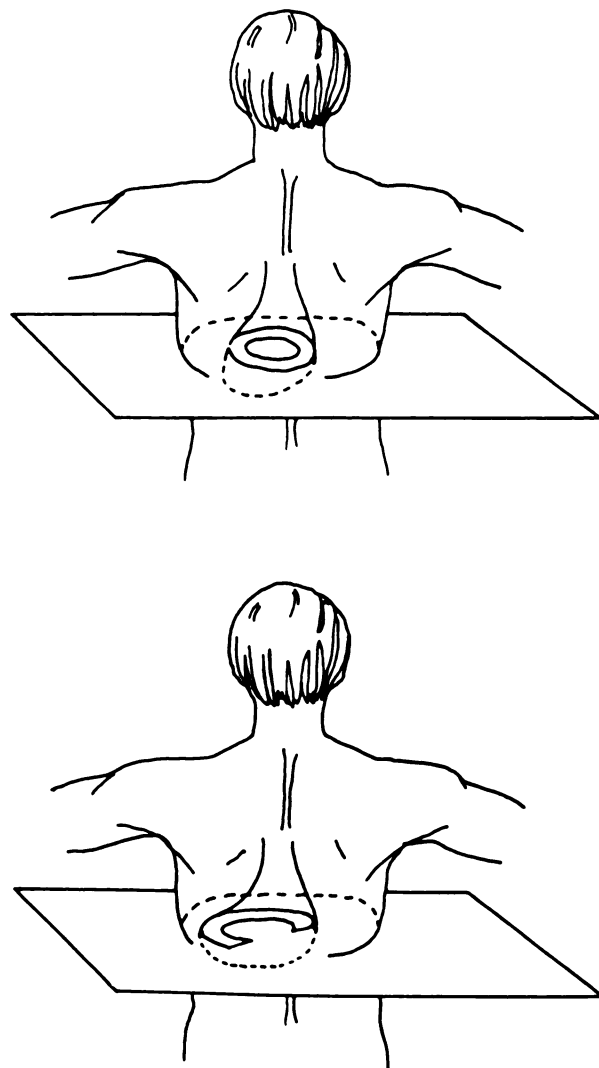


FIGURE 1
Orientation of cardiac cross-sectional tomograms as if looking down on the heart from above. The tomographic sections in patients with vertical hearts tend to be doughnut-shaped images whereas from patients with horizontal hearts appear as horseshoe-shaped images.

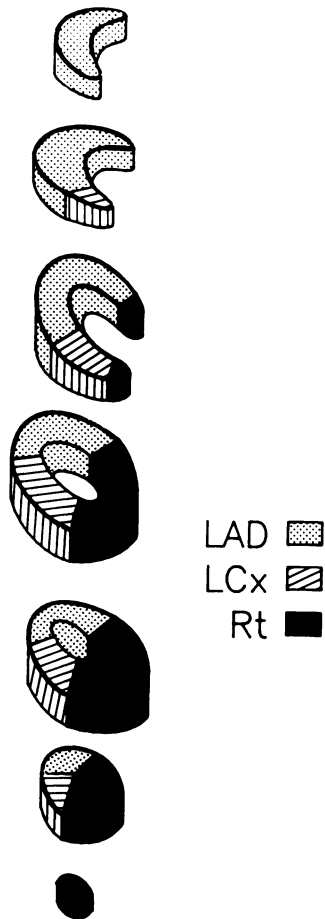


FIGURE 2
Distribution of coronary arteries on tomographic myocardial perfusion images.

each image, the left circumflex artery on the left and the right coronary artery in the inferior images. Figure 3 illustrates in the top panel that the tomographic image planes are acquired perpendicular to the long axis of the body and therefore cut the heart at an oblique semi-long axis angle, called the acquisition view. This data is then rotated into true short and long-axis views for a complete three-dimensional analysis and interpretation.

Figure 4 shows rest-stress positron emission tomography of generator produced ^{82}Rb in a patient with severe three vessel coronary artery disease in oblique semi-long axis views as acquired (panel 4A), and true short axis views (panel 4B), and in horizontal and vertical long axis views (panel 4C). Rest images are shown in the upper most of each pair of image rows (study 1). The dipyridamole stress images are in the lower row of each pair of image rows (study 2). The number after the decimal is the image plane for both study 1 and study 2. In the color coding, white indicates the highest flow, red next highest, yellow intermediate, green and blue being lowest relative flows. The tomographs in the acquisition view (panel 4A) and horizontal long axis views (top images of panel 4C) are oriented as

if looking down from above with the anterior or apex at the top of each image, the left lateral free wall on the left, and the muscular septum on the right with the AV ring and/or inferior myocardium at the bottom. In panel 4A, the first slice on the upper left shows the top of the heart while the last at the lower right shows the inferior or diaphragmatic myocardium below the left ventricular cavity. In true short-axis views of panel 4B the image planes are arranged from the AV ring at the upper left to the apex at the lower right with the anterior wall being up, the free LV wall on the left and the septum on the right of each tomograph. The open "C" in the basal short-axis views in the upper left images of panel 4B are due to the membranous septum of the left ventricular cavity which is avascular and therefore appears as a defect but reflects normal anatomy.

The resting tomographs show a small apical defect indicating a small myocardial scar. With dipyridamole stress, the anterior, septal and apical myocardium show a defect in acquisition, short and long axis views. The inferior and lateral myocardium do not show a definite stress perfusion defect on tomographic views that is identified, however, when the entire set of data are analyzed together on the polar coordinate maps.

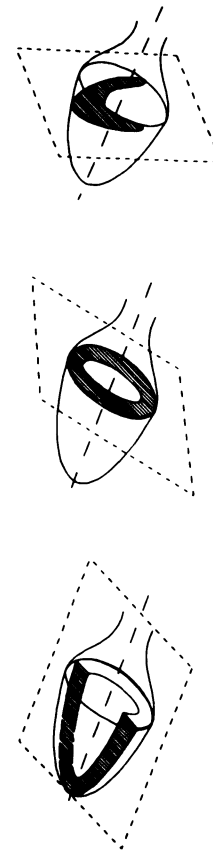


FIGURE 3
Orientation of tomographic image planes as acquired in the top panel, in true short-axis view in the middle panel and in true long-axis views in the lower panel.

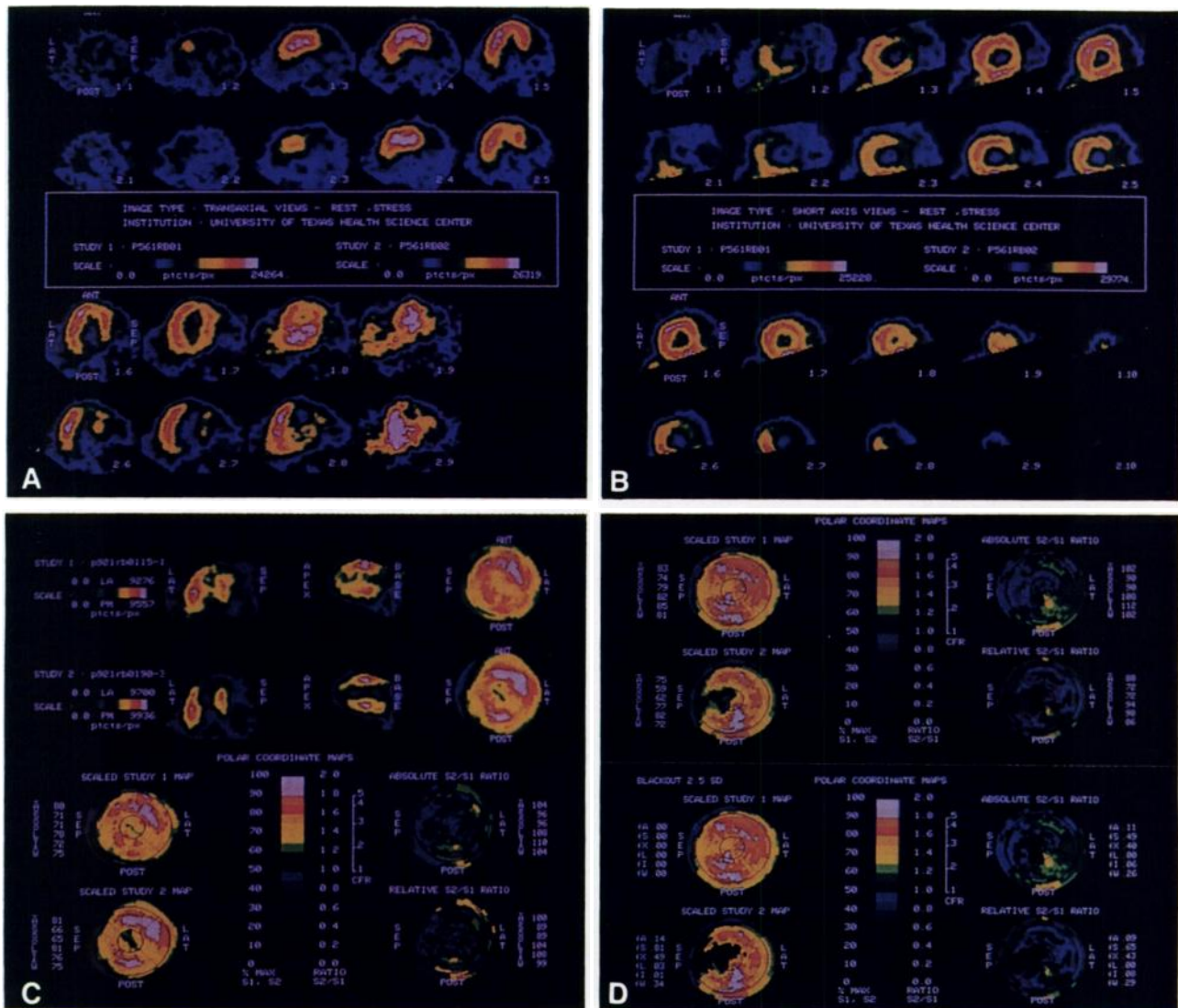


FIGURE 4 Rest-stress ^{82}Rb images of a patient with three vessel CAD. For details of the display see text, identified here as follows: *panel A* oblique, semilong-axis acquisition views; *panel B* true short-axis views, *panel C* true horizontal and vertical long-axis views with polar map displays of minimum activity in each quadrant and whole heart; *panel D* mean activity in each quadrant (upper four polar maps) and fraction of each quadrant and whole heart image outside of 2.5 s.d.s from normals (lower four polar maps).

Panel 4C shows horizontal (left) and vertical (right) long axis views of the heart. Rest images are shown in the top row with dipyridamole stress images in the lower row of the top half of the figure. The horizontal long axis views are oriented as if looking down from above. The vertical long-axis tomographs are oriented as if looking at the left side of the body cut head to toe. Anterior myocardium is at the top, inferior at the bottom, apex at the left and the AV ring on the right.

Tomographic data is summarized in a polar display as if looking at the patient from the outside toward the apex of the left ventricle located in the center of the bulls-eye with the outer rim of the bulls-eye corresponding to the AV ring. Polar displays on the left (lower half of figure) show the relative activity on a scale of 0% to 100% with rest being the upper and stress being the

lower of the polar maps on the left side of the panel. The upper right polar map (in the lower half of the figure), labeled absolute S2/S1 ratio, shows the absolute counts of the stress image divided by the rest image, displayed on a scale from 0 to 2. Increase in activity is shown by warm colors indicating ratios greater than 1 which reflect increased radiotracer uptake and perfusion due to dipyridamole. Beside the scale for absolute radiotracer uptake ratio of stress/rest is a scale of coronary flow reserve values derived by a two-compartment model accounting for extraction dependent flow and validated in animal studies. The lower right polar display, labeled relative S2/S1 ratio shows the relative distribution of flow at rest divided by the relative distribution of activity on the stress image (relative instead of absolute values), also on the scale of 0 to 2. It

therefore maps the relative change in activity from rest to stress, or the change in relative coronary flow reserve.

Letters and numbers beside each polar map show quantitative results. For regions of the heart, A = anterior, S = septal, X = apex, L = lateral, I = inferior. The numbers beside each region indicate the minimum activity as a percent of normal areas (100%). For letters with an overbar, e.g., \bar{A} , the numbers indicate mean activity rather than minimum for that quadrant of the polar map as percent of normal areas (100%) shown in Figure 4D, upper set of four polar maps. Blacked-out polar maps shown in 4D (lower set of four polar maps) demonstrate those areas that are greater than 2.5 s.d.s away from normals. For black-out figures, the numbers beside the area, i.e., fA, is the fraction of the quadrant or whole heart, fW, that is 2.5 s.d.s beyond the normal range (or 2.0 or 1.5 s.d.'s). By using a single-push-button command, the minimum, the average, or other analytic data can be instantaneously displayed beside

the appropriate polar coordinate map. The fractions, f, beyond 2.5 s.d. limits therefore provide the size of the area involved. The percent of each quadrant in short-axis views falling in 20% ranges of activity from 0-20% to 80-100% at rest and stress may also be displayed beside polar map coordinates (not shown).

The entire quantitative analysis requires 26 sec to complete on reconstructed, rotated images with each set of parameters displayed instantaneously on coded push-button command. A simple menu-driven visual interpretation can be coded in quickly while viewing the images and quantitative data beside them. Table 1 shows the printed report of all quantitative analysis for Figure 4 done automatically in addition to the visual interpretation for each quadrant in the whole heart.

For the example in Figure 4, the visual inspection of the polar map display and the quantitative analysis shows considerably more information than obtained from visual inspection of the tomographic views alone.

TABLE 1
Quantitative PET Analysis UTHSC Topet V1.1

PET NO: 561 PET ID: p561 STUDY 1: P561REST STUDY 2: P561DIPY											
ST DATE: 3/4/87 RD DATE: 8/24/88 TRACER S1: Rb TRACER S2: Rb											
READER: Gould QUALITY: Excellent											
ANGINA: Y ST: Y BKGD S1(%): 22.02 BKGD S2(%): 19.89											
T: Y AMINOPHYLLIN: Y BKGD S1(px): 7216. BKGD S2(px): 6517.											
Polar map	RGN	RGN		Regional fractions			Whole PCM		Diagnosis visual		
		min	%	1.5 s.d.	2.0 s.d.	2.5 s.d.	fractions		RGN	Inten	Size
S1	A	63	83	0.00	0.00	0.00	All regions		dA	Normal	Normal
	S	59	74	0.01	0.00	0.00	>0.8	0.45	dS	Normal	Normal
	X	67	79	0.00	0.00	0.00	>0.6	0.55	dX	Normal	Normal
	L	74	82	0.00	0.00	0.00	>0.4	0.00	dL	Normal	Normal
	I	71	85	0.00	0.00	0.00	>0.2	0.00	dI	Normal	Normal
	W	59	81	0.00	0.00	0.00	>0.0	0.00	dW	Normal	Normal
S2	A	50	75	0.31	0.16	0.14	All regions		dA	Mild	Large
	S	48	59	1.00	0.96	0.81	>0.8	0.19	dS	Severe	Large
	X	42	62	0.57	0.52	0.49	>0.6	0.51	dX	Severe	Large
	L	61	77	0.19	0.10	0.03	>0.4	0.30	dL	Mild	Large
	I	42	82	0.11	0.08	0.01	>0.2	0.00	dI	Modrt	Medium
	W	42	72	0.48	0.40	0.34	>0.0	0.00	dW	Severe	Large
S2/ S1 ABS CFR	A	0.8	1.1	0.32	0.24	0.11	MX 5%	2.83	dA	Mild	Large
	S	0.6	0.9	1.00	0.90	0.49	>1.4	0.01	dS	Severe	Large
	X	0.5	0.9	0.89	0.56	0.40	>1.25	0.03	dX	Severe	Large
	L	0.8	1.4	0.24	0.08	0.00	>1.1	0.17	dL	Mild	Large
	I	0.6	1.6	0.22	0.14	0.06	>0.9	0.48	dI	Modrt	Medium
	W	0.5	1.1	0.63	0.42	0.26	<0.9	0.31	dW	Severe	Large
S2/ S1 REL CHG	A	61	88	0.29	0.17	0.09	All regions		dA	Mild	Large
	S	42	72	1.00	0.76	0.65	>1.0	0.12	dS	Severe	Large
	X	25	72	0.55	0.48	0.43	>.66	0.63	dX	Severe	Large
	L	71	94	0.11	0.01	0.00	>.33	0.24	dL	Mild	Large
	I	31	98	0.17	0.11	0.08	<.33	0.00	dI	Modrt	Medium
	W	25	86	0.45	0.35	0.29			dW	Severe	Large

The polar map S2 shows not only a severe decrease in relative activity of the anterior, septal, apical areas but also a mild to moderate decrease in the inferior septal area not apparent on tomographic views but confirmed by the minimum activity decreasing on S2 (stress) compared to S1 (rest). The lateral wall also shows a visual and quantitative decrease in activity reflecting a mild relative decrease throughout the lateral quadrant with stress not apparent on the tomographic views. The polar map on the upper right, absolute S2/S1 ratio shows that at least one part of the heart located inferior-laterally responded with a flow reserve of 2.8 (times baseline) whereas flow reserve in the rest of the heart was severely depressed indicating three-vessel disease but worse for the LAD proximal to the first septal perforator.

In addition, parts of the anterior septum and the apex show a decrease in absolute counts with an absolute ratio of less than one on the absolute S2/S1 ratio polar map. A fall in absolute activity after dipyridamole compared to rest indicates myocardial steal and hence the presence of collaterals to viable myocardium (12, 13). The 2.5 s.d. black-out display (four-dimensional lower four polar maps) indicates that with stress (S2) 14% of the anterior wall quadrant is beyond 2.5 s.d.s of normals, 81% of the septum, 49% of the apex, and 34% of the whole heart. On the S2/S1 absolute ratio polar map, 26% of the whole myocardium shows myocardial steal and therefore viable, collateralized myocardium, mostly in the anterior, septal and apical regions. Thus, the location, intensity, size, statistical significance of, and the presence of collateralized viable myocardium can be automatically quantitated.

The two-study display format can also be used for assessing changes in two sequential stress studies for purposes of assessing regression/progression of CAD (14). Figure 5A shows long-axis views and quantitative polar displays for a *stress* image before (S1) and the *stress* image after (S2) a 6-mo period of medical therapy with no progression of symptoms or clinical event in a patient with prior painless sudden death due to CAD. However, there is obvious progression of the stress perfusion defect antero-apically and laterally confirmed by quantitative analysis in addition to a severe inferior defect also present at rest (not shown) indicating a scar. This patient therefore had severe three-vessel CAD involving an occluded right coronary artery, mild and only moderately progressive mid LAD disease and progressively very severe LCX disease. Figure 5B (upper four polar maps) shows that on the initial stress image (S1) 13% of the heart was beyond 2.5 s.d. from normals progressing on the second stress image (S2) six months later to 43% of the heart outside 2.5 s.d. Figure 5B (lower four polar maps) shows the stress perfusion image (S1) and the metabolic image using fluorine-18(¹⁸F) fluorodeoxyglucose (S2) during stress showing marked uptake laterally in the area of worsening stress defect indicating metabolic ischemia. Inferiorly there is

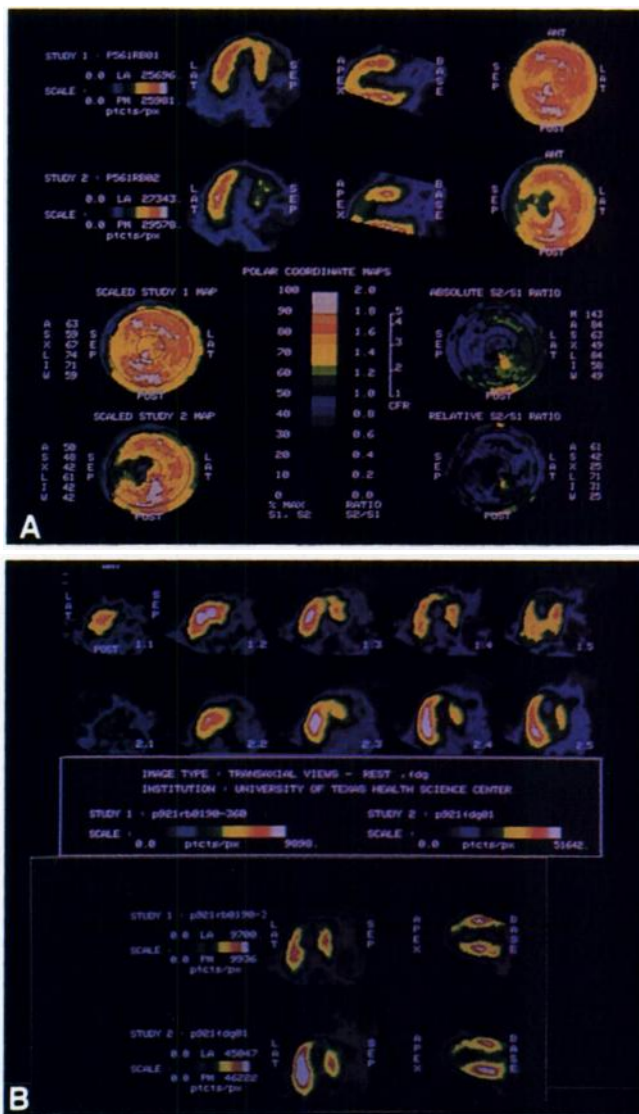


FIGURE 5 Horizontal and vertical long-axis views with quantitative polar map displays of a patient showing progression of silent CAD with worsening of anterior and lateral stress perfusion defects over a 6-mo period. Panel A shows the comparison of stress ¹³N ammonia images before (scaled study 1) and stress images after (scaled study 2) the 6-mo period with relative defect intensity displayed. The upper four polar maps of Panel B show that on the initial stress image (scaled study 1) 13% of the heart was beyond 2.5 s.d. from normals progressing to 43% of the heart 6 mo later. The lower four polar maps in Panel B compare the final stress perfusion image (scaled study 1) to the stress FDG image (scaled study 2) demonstrating a fixed inferior scar with no perfusion or FDG uptake, a severe reversible stress perfusion defect laterally that takes up FDG and therefore is viable but ischemic and a less severe anterior apical perfusion defect that does not cause ischemia since there is no glucose uptake in that area.

no perfusion or metabolic activity indicating myocardial scar. In the anterior apical region there is a moderately worsening perfusion defect but no glucose uptake indicating that the moderate impairment of

relative coronary flow reserve in the mid anterior wall did not cause ischemia. This patient had had recurrent ventricular tachycardia, controlled on anti-arrhythmics. However, with this much progression of silent coronary artery disease over a 6-mo period by PET, repeat catheterization was done showing that the LAD had progressed from a 50% to 70% diameter stenosis and the left circumflex had progressed from no stenosis to near occlusion. This example therefore demonstrates visual and quantitative progression of perfusion defects and metabolic ischemia surrounding a fixed scar, with sufficient accuracy to indicate a major intervention despite no change in symptomatic status.

Cardiomyopathy or left ventricular hypertrophy resulting from chronic hypertension typically show an enlarged heart on PET images with diffuse reduction of coronary flow reserve globally without regional defects on stress images (15). The conceptual and experimental basis for using both relative and absolute flow reserve has been previously described (16, 17) for assessing "balanced" three-vessel disease, hypertrophy, cardiomyopathy or small-vessel disease, all of which show global reduction of flow reserve without regional abnormalities (normal S2). By comparison, diffuse, even "balanced" CAD is almost always associated with regional stress perfusion abnormalities.

This laboratory has previously documented experimentally that acutely necrotic myocardium takes up ^{82}Rb but fails to trap it resulting in a "leak" out of the myocardium leaving a defect on late images (18). Consequently, for a necrotic myocardium supplied by an open coronary artery, there is initial uptake of activity reflecting adequate delivery of radiotracer followed by washout and a worsening defect on late images. For viable myocardium, there is no defect or a smaller improving defect on late images.

Figure 6 demonstrates quantitation of myocardial viability by serial imaging of a single dose of ^{82}Kb at rest in a patient who had an acute anterior myocardial infarction with a distal anterior, apical defect (S1) indicating an initial mid LAD occlusion. Figure 6A shows the early Rb image from the first 15 to 90 sec of data (S1) and the late Rb image from 90 to 360 sec of data (S2). There is a mild distal anterior apical defect early (S1) that washed out leaving a more severe defect on the late image (S2). These results indicate that the LAD spontaneously reperfused. The mid-anterior subendocardium and apex are necrotic, since they don't retain rubidium but there is a substantial amount of the distal anterior epicardium that does retain rubidium indicating viability.

This assessment of viability from a single resting injection of ^{82}Rb with serial list mode imaging are compared to the F-18 fluorodeoxyglucose image (after glucose loading), in Figure 6B. The late rubidium image is shown in S1 with a substantial rim of anterior activity indicating viable tissue. This image is identical to FDG

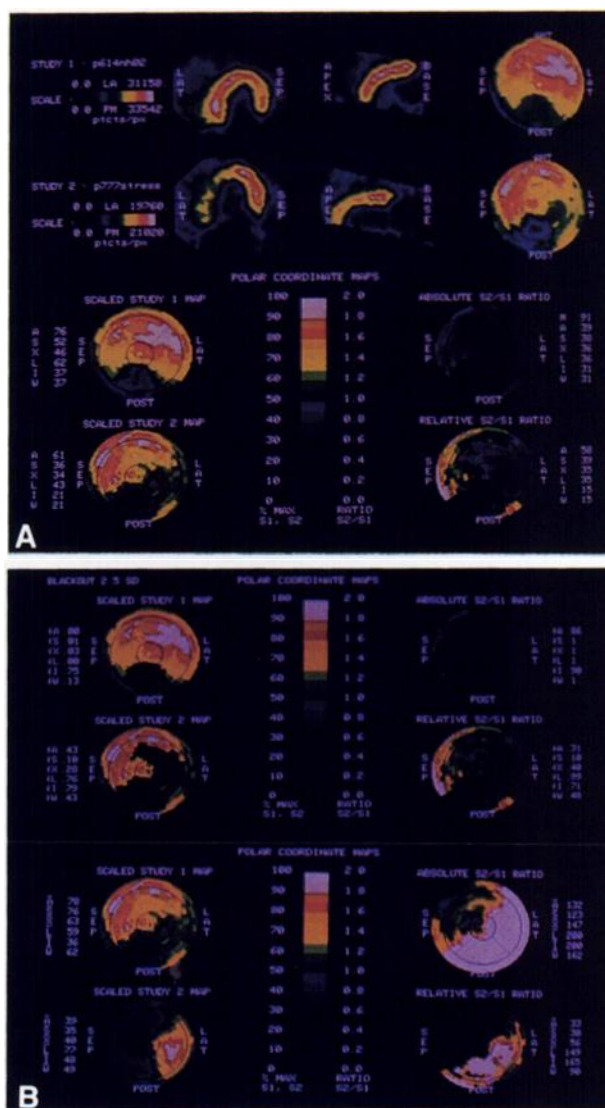


FIGURE 6 Serial perfusion imaging after a single injection of ^{82}Rb at rest. Panel A shows long-axis views early (scaled study 1) and late (scaled study 2) showing washout anterior and apically indicating necrosis but also substantial Rb trapping in the distal anterior wall indicating substantial viable myocardium. Panel B compares the resting, late ^{82}Rb image (upper of paired rows) to the resting FDG image (lower of paired rows) showing them to be identical, both reflecting myocardial viability.

image (S2) also showing an anterior rim of uptake indicating viability with a necrotic apex and subendocardium. Thus, viability can be assessed by a single list mode study using generator produced ^{82}Rb without the cyclotron necessary for FDG.

DISCUSSION

Although first to report surface maps for three-dimensional display of cardiac PET (19), we have developed tomographic and polar map presentations for

routine clinical use because they are familiar to viewers and more readily accepted. For PET to be used as a clinical tool instead of for research purposes only as in the past, image presentation and data analysis have to become more automated. To achieve volume throughput and standardization of intensity levels in quantification, user interaction must be minimized, particularly for clinical work by personnel without years of PET experience. Therefore, the display and analysis methods reported here were not intended to be innovative or new per se but to be familiar, commonplace, and routine in order to demonstrate that an esoteric, complex and previously research oriented technology could be applied for routine clinical studies.

The first innovation in our development of standard polar map analysis is applying the concepts of relative and absolute coronary flow reserve (16, 17) to clinical studies by PET. Absolute and relative coronary flow reserve are independent, complementary variables providing, together, a more complete measure of functional stenosis severity than either one alone (16, 17). Absolute flow reserve reflects the flow capacity of the coronary vascular bed under whatever conditions of pressure, workload or stenoses are present. It reflects the global summed effects of these various factors including stenoses without being specific for the mechanism or cause of altered flow reserve. Relative maximum coronary flow or relative flow reserve reflects more specifically the effects of the stenosis independent of and not affected by the other physiologic variables if normal maximum flow is high enough. Thus, absolute and relative coronary flow reserve are complimentary because absolute flow reserve demonstrates whether an adequate flow response occurred (as reflected by the polar map absolute S2/S1 ratio) and identifies diffusely impaired flow reserve as seen in cardiomyopathy, LVH, small-vessel disease or "balanced" three-vessel coronary atherosclerosis; relative flow reserve reflects stenosis severity independent of varying aortic pressure and workload (as shown by S2 and relative S2/S1 ratio polar maps) while failing to reflect globally reduced flow reserve (16, 17). From its conception in our laboratory 15 years ago (20), this assessment of physiologic stenosis severity has evolved from a basic laboratory observation to clinical utility.

The other innovation in our approach is the development of attenuation corrected quantitative PET data into a clinically applicable format. These quantitative methods are the first application of cardiac PET in non-University cardiologic practice beginning in March of 1988 (21, 22) with now over 600 patients studied in private practice since that time. Therefore, the method we report is a familiar, accepted display of quantitative PET data integrating basic physiologic concepts and complex technology for identifying and assessing severity of CAD.

However, there are some qualifications or limitations to this approach. Based on our experience in ~800 university-based clinical studies, it is necessary to utilize all views available for interpretation—the acquisition, short-axis, long-axis, and polar map views together. Short-axis views alone commonly fail to show abnormalities seen on long-axis views. For "balanced" three-vessel CAD, the polar map display showing all of the data from the heart demonstrate abnormalities more accurately than any of the tomographic views alone.

The polar display also distorts the spatial anatomy so that the visual impression of size on the polar map does not always correspond to the actual size of myocardium involved. Accordingly, the percent of myocardium outside chosen standard deviation limits is calculated from the true short-axis views and not from the polar map display. It is also our impression that processing PET data with software designed for SPECT imaging having different filters, rotational algorithms etc. that are optimized for SPECT are less satisfactory for PET images. Although the diagnostic accuracy of PET data processed by SPECT software is better than by SPECT imaging (23, 24), PET images processed with SPECT software appear to be overly smooth with data potentially displaced into neighboring pixels by multistep rotational schemes or excessive smoothing. Despite specificity of PET for diagnosis of CAD being much higher than for SPECT (23–25), sensitivity in those studies was comparable to SPECT. The explanation is that suboptimal processing of PET data by SPECT software (23, 24) in our experience lowers diagnostic content in comparison to software specifically designed for PET reconstruction and analysis with which higher diagnostic accuracy is obtained (2, 4, 21). Another reason for lower sensitivity (or specificity) is inadequate total counts in the whole heart image set. Six million counts per whole heart image set, as reported with a block camera design having high deadtime losses (25), seriously compromises diagnostic content for short lived tracers like ^{82}Rb or ^{15}O water. By comparison, for ^{82}Rb we acquire ~15 million counts per whole heart data set and achieve a greater sensitivity and specificity. In count poor studies, summing slices makes them look better but doesn't overcome the basic inaccuracy due to inadequate counts in the whole heart data set.

Finally, all models for determining absolute myocardial perfusion or absolute coronary flow reserve require measurement of the arterial input function. While feasible in a research laboratory, measurement of arterial input function is only now being developed for routine clinical use. Fortunately, cardiac output increases on the average only 50% over resting conditions during dipyridamole stress (26) as compared to three to four times increase for treadmill stress. This mean increase of 50% in cardiac output by dipyridamole is built into the mathematic model used for calculating absolute

coronary flow reserve in our quantitative method. As the measurement of arterial input is reduced to a clinical routine, individual variation of cardiac output or arterial input function during dipyridamole stress can be accounted for with further improvement in measuring absolute coronary flow reserve.

ACKNOWLEDGMENTS

This work was supported in part by NIH Grants, RO1-HL26862, RO1-HL26885, Grant DE FG05-84ER60210 and as a joint collaborative project with the Clayton Foundation for Research.

The authors thank Mary Haynie, RN, and Mary Jane Hess, RN, for their technical assistance.

REFERENCES

- Schelbert HR, Wisenberg G, Phelps ME, et al. Non-invasive assessment of coronary stenoses by myocardial imaging during pharmacologic coronary vasodilation. VI. Detection of coronary artery disease in human beings with intravenous N-13 ammonia and positron computed tomography. *Am J Cardiol* 1982; 49:1197-1207.
- Gould KL, Goldstein RA, Mullani NA, et al. Noninvasive assessment of coronary stenoses by myocardial perfusion imaging during pharmacologic coronary vasodilation. VIII. Clinical feasibility of positron cardiac imaging without a cyclotron using generator-produced rubidium-82. *J Am Coll Cardiol* 1986; 7:775-789.
- Tamaki N, Yonekura Y, Senda M, et al. Myocardial positron computed tomography with ¹³N-ammonia at rest and during exercise. *Eur J Nucl Med* 1985; 11:246-251.
- Demer LL, Gould KL, Goldstein RA, et al. Assessment of coronary artery disease severity by positron emission tomography: comparison with quantitative arteriography in 193 patients. *Circulation* 1989; 79:825-835.
- Gould KL. Identifying and measuring severity of coronary artery stenosis—quantitative coronary arteriography and positron emission tomography. *Circulation* 1988; 78:237-245.
- Goldstein RA, Kirkeeide R, Demer LL, et al. Relations between geometric dimensions of coronary artery stenoses and myocardial perfusion reserve in man. *J Clin Invest* 1987; 79:1473-1478.
- Garcia EV. Quantitative rotational thallium-201 myocardial tomography. *J Nucl Med* 1985; 26:17-26.
- DePasquale EE, Nody AC, DePuey EG, et al. Quantitative rotational thallium-201 tomography for identifying and localizing coronary artery disease. *Circulation* 1988; 77:316-327.
- Mullani NA, Gould KL. First pass regional blood flow measurements with external detectors. *J Nucl Med* 1983; 24:577-581.
- Mullani NA, Goldstein RA, Gould KL, Fisher DJ, Marani SK, O'Brien HA. Myocardial perfusion with rubidium-82. I. Measurement of extraction fraction and flow with external detectors. *J Nucl Med* 1983; 24:898-906.
- Mullani NA, Goldstein RA, Gould KL, Fisher DJ, Marani SK, O'Brien HA. Myocardial perfusion with rubidium-82. II. The effects of metabolic and pharmacologic interventions. *J Nucl Med* 1983; 24:907-915.
- Demer LL, Gould KL, Kirkeeide RL. Assessing stenosis severity: Coronary flow reserve, collateral function, quantitative coronary arteriography, positron imaging, and digital subtraction and angiography. A review and analysis. *Prog Cardiovasc Dis* 1988; 30:307-322.
- Demer LL, Goldstein R, Mullani N, et al. Coronary steal by non-invasive PET identifies collateralized myocardium. [Abstract] *J Nucl Med* 1986; 27:977.
- Demer LL, Kirkeeide RL, Haynie MP, et al. Feasibility of following progression/regression of coronary artery stenosis by positron emission tomography during dipyridamole-hand grip stress. *Circulation* 1987; 76:IV 4.
- Goldstein RA, Haynie M, Gould KL. Limited myocardial perfusion reserve in patients with left ventricular hypertrophy. *Clin Res* 1988; 36:279A.
- Kirkeeide RL, Buchi M, Gould KL. Coronary flow reserve as a physiologic measure of stenosis severity. Part I. Relative and absolute flow reserve during changing aortic pressure and cardiac workload. *J Am Coll Cardiol*: in press.
- Kirkeeide RL, Buchi M, Gould KL. Coronary flow reserve as a physiologic measure of stenosis severity. Part II. Determination from arteriographic stenosis dimensions under standardized conditions. *J Am Coll Cardiol*: in press.
- Goldstein RA. Kinetics of rubidium-82 after coronary occlusion and reperfusion. *J Clin Invest* 1985; 75:1131-1137.
- Kehtarnavaz N, DeFigueiredo RJP. A novel surface reconstruction and display method for cardiac PET imaging. *IEEE Trans Med Imag* 1984; MI-3:108-115.
- Gould KL, Lipscomb K, Hamilton GW. Physiologic basis for assessing critical coronary stenosis. *Am J Cardiol* 1974; 33:87-94.
- Williams BR, Jansen DE, Wong LF, Fiedotin AF, Knopf WD, Toporoff SJ. Positron emission tomography for the diagnosis of coronary artery disease: a non-university experience and correlation with coronary angiography [Abstract]. *J Nucl Med* 1989; 30:845.
- Lyle FM, Gordon DG. The importance of timing with Rb-82 PET imaging of the heart [Abstract]. *J Nucl Med* 1989; 30:871.
- Marwick TH, Go RT, MacIntyre WJ, et al. Disparities between myocardial perfusion imaging using Rb-82 PET and Tl-201 SPECT after dipyridamole stress [Abstract]. *J Nucl Med* 1989; 20:861.
- Go RT, Marwick TH, MacIntyre WJ, Rehm PK, Underwood DA, Saha GB, Simpfendorfer CC. Initial results of comparative rubidium-82 and thallium-201 myocardial perfusion imaging in diagnosis of CAD [Abstract]. *J Nucl Med* 1989; 30:759.
- Kalus ME, Stewart RE, Gacioch GM, Squicciarini SA, Hutchins GD, Kuhl DE, Schwaiger M. Comparison of Rb-82 PET and Tl-201 SPECT for the detection of regional coronary artery disease [Abstract]. *J Nucl Med* 1989; 30:829.
- Brown G, Josephson MA, Peterson RB, et al. Intravenous dipyridamole combined with isometric hand-grip for near maximal acute increase in coronary flow in patients with coronary artery disease. *Am J Cardiol* 1981; 48: 1077-1085.